Structural transitions and magnetic response of supramolecular magnetic polymerlike structures with bidisperse monomers

Ekaterina V. Novak [ORCID],[*] Elena S. Pyanzina [ORCID], and Marina A. Gupalo

Institute of Natural Sciences and Mathematics, Ural Federal University, Ekaterinburg 620083, Russian Federation

Norbert J. Mauser

Research Platform MMM Mathematics-Magnetism-Material, c/o Faculty of Mathematics, University of Vienna, 1090 Vienna, Austria

Sofia S. Kantorovich [ORCID][†]

Faculty of Physics, Computational and Soft Matter Physics, University of Vienna, 1090 Vienna, Austria

Supramolecular magnetic polymerlike (SMP) structures are nanoscaled objects that combine the flexibility of polymeric conformations and controllability of magnetic nanoparticles. The advantage provided by the presence of permanent cross-linkers is that even at high temperature, a condition at which entropy dominates over magnetic interactions, the length and the topology of the SMP structures are preserved. On cooling, however, preexistent bonds constrain thermodynamically equilibrium configurations, making a low-temperature regime for SMP structures worth investigating in detail. Moreover, making SMP structures with perfectly monodisperse monomers has been a challenge. Thus, the second open problem in the application of SMP structures is the missing understanding of the polydispersity impact on their structural and magnetic properties. Here extensive Langevin dynamics simulations combined with parallel tempering method are used to investigate SMP structures of four different types, i.e., chainlike, Y-like, X-like, and ringlike, composed of monomers of two different sizes. Our results show that the presence of small particles in SMP structures can qualitatively change the magnetic response at low temperature, making those structures surprisingly more magnetically responsive than their monodisperse counterparts.

I. INTRODUCTION

The combination of polymers and micro- or nanoparticles is one of the most successful available approaches for the design of novel materials with highly tunable properties [1,2]. One of the ways to realize this potential is to create supramolecular polymerlike structures in which the part of monomers is played by nanoparticles. The controllability of these structures can be achieved by using magnetic nanoparticles, profiting this way not only from the response of the monomers to an applied magnetic field, but also from intrinsic magnetic intermonomer interactions. The potential of supramolecular magnetic polymerlike (SMP) structures in microfluidics and biomedical applications has been already recognized [3–5]. In order to capitalize on this potential, a fundamental understanding of the interplay between monomer size, cross-linking, and SMP topology on one side and magnetic, structural, and rheological responses on the other is required.

Linear SMP structures, i.e., magnetic filaments (MFs), have been targeted and actively studied for more than 20 years by now [6–23]. Magnetic filaments with monomers in the micrometer range were synthesized more than one decade ago [24]. Today a plethora of synthesis techniques is available to create MFs [15,22,25–35]. All those techniques, albeit powerful and promising, still cannot fully guarantee the monodispersity of the magnetic monomers.

Theoretical and computational studies of variously shaped SMP structures can be divided into two large groups. In one, MFs are considered flexible magnetic objects, in which individual magnetic monomers are not resolved [36–42]. Those works are particularly useful when describing deformations in flow or explaining the interplay between applied rotating fields and hydrodynamics [43]. When applied to nanoscale objects, such an approach lacks the effects of thermal fluctuations and the resolution of the possible structural transitions caused by monomer-monomer interactions. Finally, traditionally, the magnetization is assumed to be uniform along the backbone of the elastic rod, thus not allowing for the effects of monomer polydispersity.

The other group of theoretical works, in contrast, explicitly models the monomers [44–46]. These approaches allow us to account for monomers of different shapes and to scrutinize both structural and magnetic response of SMP structures [47,48] as well as brushes made of the latter [49].

---

[*]ekaterina.novak@urfu.ru

[†]Also at Institute of Natural Sciences and Mathematics, Ural Federal University, Ekaterinburg 620083, Russian Federation and Research Platform MMM Mathematics-Magnetism-Material, University of Vienna, 1090 Vienna, Austria.

In these approaches hydrodynamics can be considered [50], however on a scale smaller than that treated by the formalism mentioned in the preceding paragraph. Although useful to describe monomer-monomer interactions and their impact on the macroscopic behavior of the SMP structures, all known monomer-based SMP studies operate exclusively systems with identically sized magnetic nanoparticles [51,52].

The intrinsic polydispersity of magnetic nanoparticles is known to dramatically influence magnetic [53–55], scattering [56,57], rheological [58], elastic [59], and transport [60] properties of magnetic soft materials as the magnetization of typically used single-domain magnetic nanoparticles is directly proportional to their volumes. Hence, it is natural to expect that the properties of the SMP structures would be altered as well if the monomers of different sizes were present in the systems.

Previously, it was shown that considering magnetic particles of two different sizes could shed light on the polydispersity effects on structural transitions and macroscopic responses of materials containing them [55,59,61–63]. Following this strategy, here we employ molecular dynamics computer simulations to investigate structural transitions in SMP structures with bidisperse monomers of four different topologies: linear and Y, X, and ring shaped. We use temperature as a control parameter in order to understand if the presence of smaller in size and magnetization monomers can affect the closure of magnetic flux in these systems on cooling. Such a closure was previously shown to lead to the formation of magnetically inert structures [64] that however can be used as potential containers for cargo in micro- and nanofluidics devices.

The paper is organized as follows. In Sec. II we describe the model and the methods employed. The description of the results, provided in Sec. III, is split into two steps: First, the temperature dependences of the total magnetization and gyration radii of the SMP structures are discussed, and then, increasing the resolution, we carefully describe structural transitions in SMP structures on the level of monomers. Section IV concludes the paper with a brief summary of the results and an outlook for future work.

II. SIMULATION MODEL AND METHODS

We consider SMP structures formed by N ferromagnetic particles of two different sizes: small and large monomers are modeled as spherical soft beads of characteristic diameters $\sigma_s = 1$ and $\sigma_l = 1.6$ correspondingly, carrying point magnetic dipoles $\vec{\mu}_s$ and $\vec{\mu}_l$ at their centers. Any two monomers i and j at a distance $r = |\vec{r}_{ij}|$ interact with each other via a purely repulsive Weeks-Chandler-Andersen pair potential [65]

$$U_{\text{WCA}}(i, j) = \begin{cases} 4\epsilon\left[\left(\frac{\sigma_i+\sigma_j}{2r}\right)^{12} - \left(\frac{\sigma_i+\sigma_j}{2r}\right)^{6} + \frac{1}{4}\right], & r < r_{\text{cut}} \\ 0, & r \geqslant r_{\text{cut}}, \end{cases}$$

(1)

where ϵ is the energy scale of repulsion and $r_{\text{cut}} = 2^{-5/6}(\sigma_i + \sigma_j)$. Each pair of magnetic dipoles $\vec{\mu}_i$ and $\vec{\mu}_j$ experiences the conventional long-range dipole-dipole pair interaction

$$U_{\text{dip}}(i, j) = \frac{\vec{\mu}_i \cdot \vec{\mu}_j}{r^3} - \frac{3[\vec{\mu}_i \cdot \vec{r}_{ij}][\vec{\mu}_j \cdot \vec{r}_{ij}]}{r^5}.$$
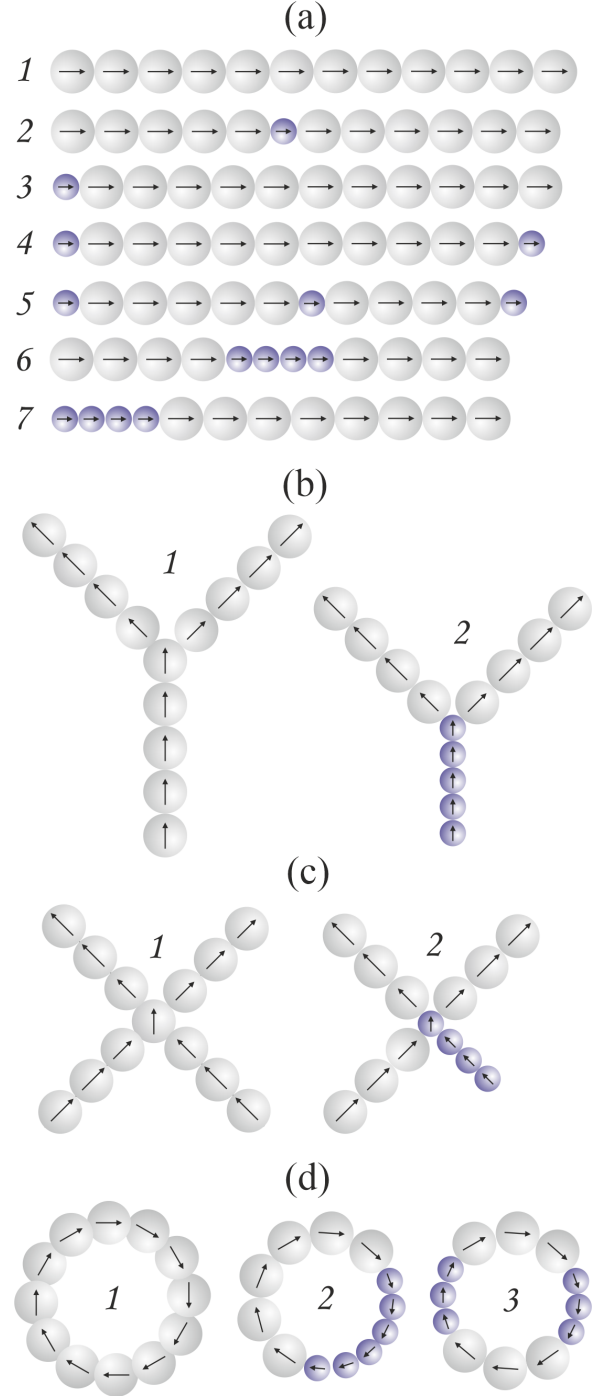
(2)

FIG. 1. Sketch of all investigated topologies: (a) open chains, (b) Y's, (c) X's, and (d) rings.

Figure 1 shows all investigated topologies. Of course, there is a plethora of possibilities to mix small and large particles inside the MFs. One would however expect the main difference for the situation of a small particle (particle segment) to be between forming an open end of the structure or being inside it. We have seven different configurations of open chains [Fig. 1(a)]. All chains consist of 12 beads. For case 1, all particles in the chain are large. The second type of chain includes one small particle in the middle of the chain. In type 3, the small particle is placed at the chain end. The fourth
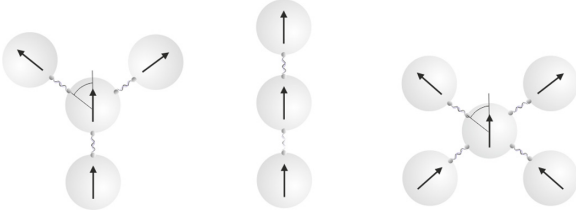
FIG. 2. Springs attached to the surface of the particles for different types of connections. In the case of a Y-like SMP structure (left), the junction has an opening of $120°$, while for an X-like SMP structure (right) the opening angle is $90°$; linear segments are cross-linked head to tail.

configuration consists of a chain of ten large particles with two small particles attached to its ends. The fifth type of chain includes nine large beads and three small ones: two at the ends and one in the middle. Types 6 and 7 contain a four-small-particle segment inside and on the edge, respectively. In contrast to chains, only one case in addition to the monodisperse Y-like SMP structure is investigated, with one arm made of small particles [Fig. 1(b)]. The arm made of small particles includes small particles in the center of the structure and at an open end. The behavior of the latter can be compared to the other two ends made of large particles. In the case of X-like SMP structures [Fig. 1(c)], two similar cases are investigated: a purely monodisperse one used as a reference and a SMP structure with one arm fully made of small monomers. In addition to a reference monodisperse 12-particle ringlike SMP structure, we consider two other configurations with six small particles each, either being subsequently connected to each other or split into two segments of length 3 [Fig. 1(d)], as a ring has no open ends. We opt for fixing nearly the same total number of particles in SMP structures in order for them to give comparable saturation magnetization, even though X-like and chainlike SMP structures in this case have substantially different entropies.

All those structures are realized by cross-linking neighboring monomers by finitely extensible nonlinear elastic (FENE) springs [66]

$$U_{\text{FENE}}(r; K, r_{\max}) = -\frac{1}{2} K r_{\max}^2 \ln \left[1 - \left(\frac{r}{r_{\max}} \right)^2 \right], \quad (3)$$

where $K = 10$ defines the elastic strength of the bond and $r_{\max} = 0.75(\sigma_i + \sigma_j)$ its maximum extension. The springs are attached to the surface of the particles as shown for different types of connections in Fig. 2. The choice of $r_{\max}$ does not affect equilibrium conformations but allows us to use a relatively large time step. This cross-linking correlates the orientation of the magnetic moment and the SMP backbone and penalizes not only translations, but also rotations of the monomers.

All simulations mentioned in this paper are carried out in ESPResSo 4.1.4 [67]. As usual in simulations with mesoscale models, we use a set of reduced, i.e., dimensionless, units.

Here we define lengths and masses in units of the diameter and mass of the small monomer, so we take $\sigma_s = 1$ and $m_s = 1$. The energy scale ϵ and the magnetic interaction strength μ^2 are measured in units of dimensionless thermal energy T,

with the Boltzmann constant k set to unity. In our case, $T = 1$ corresponds to room temperature conditions. The parameter ϵ is fixed to unity throughout the work. There are several ways to investigate the effects of magnetic coupling strength on the SMP behavior. Here we choose to fix particle magnetic moments so that $\mu_s^2/(T \sigma_s^3) = 1.3$ and $\mu_l^2/(T \sigma_l^3) = 5.32$ at $T = 1$, with $\sigma_l = 1.6$. Thus, the only parameter we vary is the dimensionless temperature T from 0.2 to 5. In a real experiment this range means changing the magnetic material and/or size of magnetic nanoparticles: For temperature above 0.6 this can be provided by magnetite in a range between 10 and 35 nm, while for lower temperatures the model corresponds to monomers made of cobalt.

The parameters described above are sampled by performing molecular dynamics simulations with a Langevin thermostat. This means that the motion of each bead i is governed by the translational and rotational Langevin equations, obtained by adding the stochastic and friction terms to the Newtonian equations

$$m_i \left(\frac{d\vec{v}_i}{dt} \right) = \vec{F}_i - \Gamma_{\mathrm{T}} \vec{v}_i + \vec{\xi}_{i,\mathrm{T}}, \quad (4)$$

$$\bar{I}_i \left(\frac{d\vec{\omega}_i}{dt} \right) = \vec{\tau}_i - \Gamma_{\mathrm{R}} \vec{\omega}_i + \vec{\xi}_{i,\mathrm{R}}, \quad (5)$$

where $\vec{F}_i$ and $\vec{\tau}_i$ are the total force and torque acting on the particle, respectively, and m_i is the particle mass and $\bar{I}_i$ its inertia tensor. Finally, Γ_{T} and Γ_{R} are the translational and rotational friction constants and $\vec{\xi}_{i,\mathrm{T}}$ and $\vec{\xi}_{i,\mathrm{R}}$ are the Gaussian random force and torque, respectively, fulfilling the normal fluctuation-dissipation rules. In this work we used unitary inertia tensors as they provides fast convergence; we focus exclusively on thermodynamic equilibrium. For the same reason, the friction terms in Eqs. (4) and (5) can be chosen arbitrarily. We choose $\Gamma_{\mathrm{T}} = 1$ and $\Gamma_{\mathrm{R}} = \frac{3}{4}$ as values known for providing a fast relaxation in this type of simulation [62,68]. Masses of all particles are fixed to unity. This approach treats implicitly the effects of the thermal fluctuations of the background [66,69]. Equations (4) and (5) are integrated by means of a velocity Verlet scheme. No periodic boundary conditions are used and each simulation run contains only one SMP structure in a simulation box whose side is fixed to $30\sigma_s$. All forces and torques are calculated directly; no cutoff radii are employed. FENE springs are attached with the help of virtual sites, special particles whose equations of motion are not integrated, and all force and torques acting on them are translated to the centers of mass of the real particles they belong to [67].

The simulation protocol consists of a warmup of the initial configurations at $T = 2$, performing 2×10^3 integration steps with a time step $\delta t = 10^{-3}$. Finally, a production cycle of 3×10^6 steps is performed.

Here we used the replica exchange molecular dynamics method [70,71] to improve the statistics and prevent the system from getting trapped in a local minimum. In this method, $L = 50$ independent simulations of the same system are run simultaneously, each with one value of a given parameter T_i, with i from 1 to L. After equilibration of each replica, we exchange the two neighboring configurations using the Boltzmann probability. This exchange series demands the energy
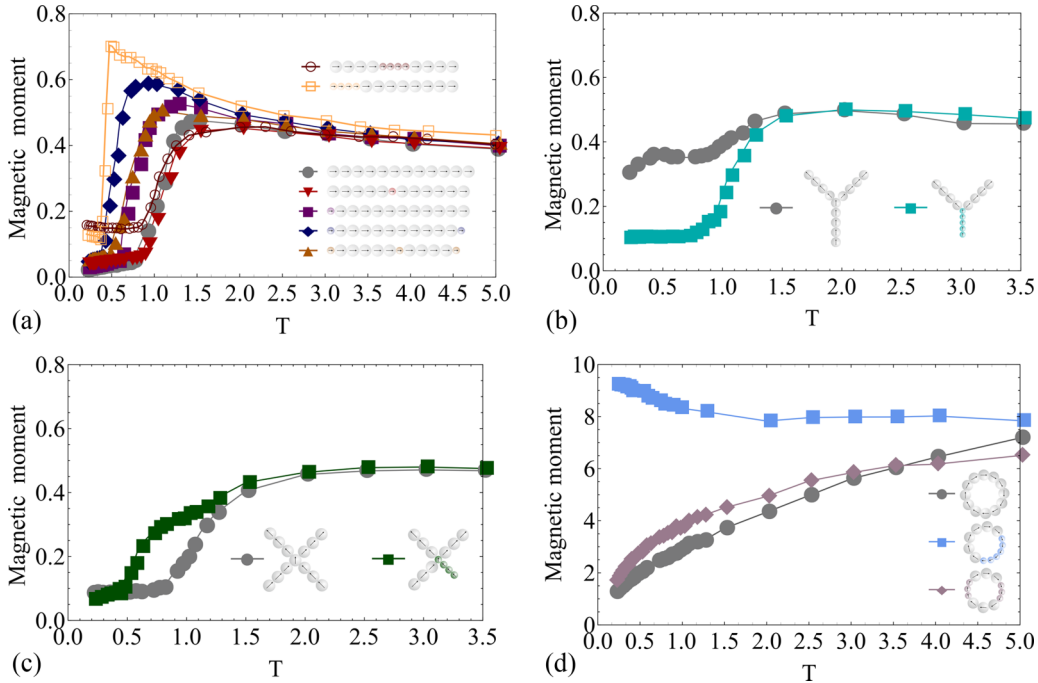
FIG. 3. Magnetic moment as a function of T: (a) chainlike SMP structures, (b) Y-like SMP structures, (c) X-like SMP structures, and (d) ringlike SMP structures. The content and the positioning of small monomers are provided in the legend.

histograms of neighboring simulations to have a substantial overlap in order to be effective. To balance the accuracy of the algorithm and the computational cost, we choose sets of parameter values that provide overlaps of about 30% of the histogram areas.

III. RESULTS AND DISCUSSION

A. Magnetization and radii of gyration

We start the analysis of the data by looking at the modulus of a total magnetic moment of a SMP structure, i.e., the vector sum of all monomer moments, as a function of T. The results are presented in Fig. 3. All plots but those in Fig. 3(d) are normalized by the magnetization of the initial configuration shown in Fig. 1. In the case of rings, the initial configuration has a zero magnetic moment; hence here the normalization is done by $\mu = 1$. All the plots are obtained by averaging the data over 1000 snapshots. The error bars are smaller than the symbol size.

It is known that non-cross-linked monodisperse magnetic nanoparticles tend to form first chains and open branched structures on cooling that close into rings with vanishing total magnetic moment under further temperature decrease [64]. At the same time, it is known that particle polydispersity leads to a significant reduction of the cluster size and prevents ring formation (see [63] and references therein). Here, in the behavior of the chainlike SMP structures' total magnetic moment, presented in Fig. 3(a), we see a clear competition between the two factors. Thus, if looking from the right to the left, following the cooling, the monodisperse SMP structures' magnetization start falling earlier than those of the SMP structures with small particles. The most prominent difference is observed for the chains that contain small particles at the ends (yellow open squares and blue rhombuses). In fact, the magnetization

clearly exhibits a maximum at the temperature where the magnetization of all other SMP structures is already decreasing rapidly. Interestingly enough, the presence of a small particle in the middle of the chain with two small particles at the ends (orange triangles) facilitates magnetization decay and the magnetic moment behaves similarly to that of a chain with a small particle at only one end (closed magenta squares). Moreover, if we consider the chains with small particles in the middle (open red circles and closed red triangles), then their magnetization behavior initially looks very similar to the monodisperse case [gray circles in Fig. 3(a)]. On cooling, however, the presence of a small-particle segment inside the chain leads to a slower decay of the total magnetic moment. Looking at Figs. 3(b) and 3(c), we can see how the presence of the small-particle arm impacts the decrease of the total magnetization. For Y-like structures for the studied region of T none of the curves reach zero. Moreover, for values of T where the Y-like SMP structure with a small-particle arm shows a plateau (cyan squares), in the monodisperse case, there is a local maximum and the overall values are higher. In contrast to Y-like SMP structures, but similarly to linear ones, X-like SMP structures with a small-particle arm exhibit slower magnetization decay on cooling and develop a shoulder near $T \sim 0.5$. We find qualitatively different behavior for ringlike SMP magnetization, plotted in Fig. 3(d). Initial configurations in this case are ideal rings that have zero total magnetization. Thermal fluctuations at high T lead to a finite value that for monodisperse rings (gray circles) monotonically goes to zero on cooling. If small particles are mixed in so that segments of three like-sized particles are alternating (bordeaux rhombuses), the decrease is slightly hindered, but retains its profile. The magnetization on the contrary grows on cooling however, if small particles are forming a single sequential segment (blue squares).
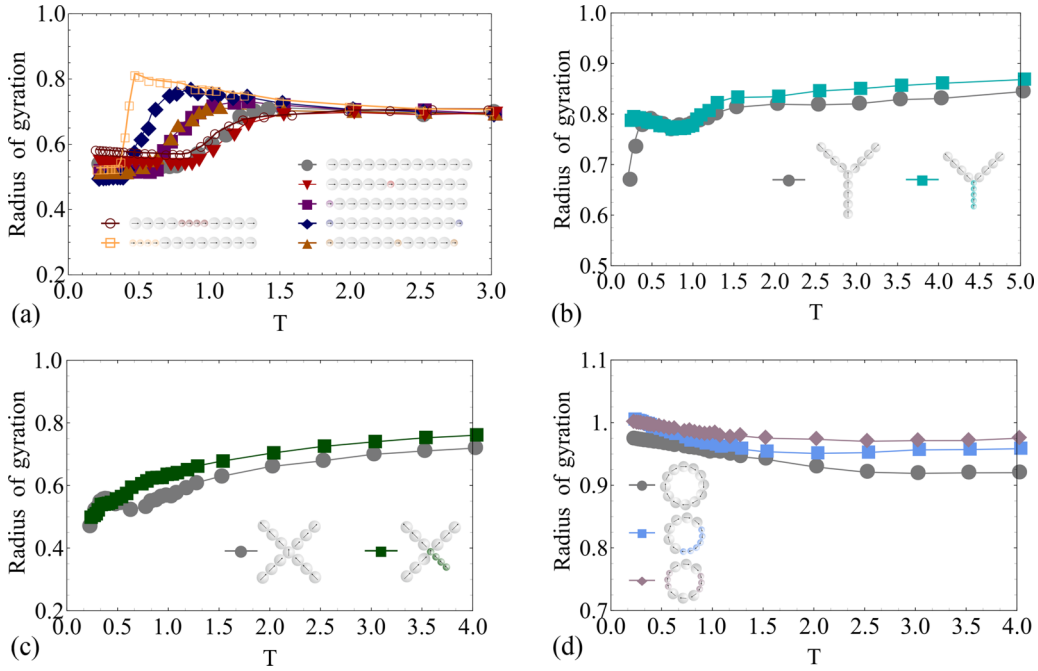
FIG. 4. Radius of gyration as a function of T: (a) chainlike SMP structures, (b) Y-like SMP structures, (c) X-like SMP structures, and (d) ringlike SMP structures. The content and the positioning of small monomers are provided in the legend.

In order to clarify the observed differences between different topologies and scrutinize the impact of small particles on the properties of SMP structures, in Fig. 4 we plot the temperature dependence of gyration radii R_g,

$$R_g = \left[\frac{1}{N_p} \sum_{i=1}^{N_p} (\vec{r}_i - \langle \vec{r} \rangle)^2 \right]^{1/2}, \qquad (6)$$

where $\langle \vec{r} \rangle = \sum_{k=1}^{N_p} \vec{r}_k / N_p$ for different types of SMP structures. We normalize R_g by its value in the initial configuration, similarly to the previously discussed magnetic moment. The only difference is that in Fig. 4 the plots for rings are also normalized by the corresponding value of R_g in the initial state. In Fig. 4(a) we notice that independently the structure of the chainlike SMP structure at low temperature, the normalized gyration radius converges to approximately half of that in the initial fully stretched configuration. The way R_g reaches its limiting low-T value, however, dramatically depends on the presence of small particles. Similarly to the magnetization in Fig. 3(a), if small particles are attached to the chain ends, the decay of the R_g not only is slowed down on cooling, but has even a local maximum at $T \sim 0.7$ for the case of two small particles (blue rhombuses) and at $T \sim 0.5$ if a small-particle segment forms an open chain end (open yellow squares). In the case of one small particle at the end or of two small particles at the ends and one in the middle of a linear SMP structure (bordeaux squares and orange triangles respectively), the local maximum of R_g shifts to higher values of T and goes down in height. As for magnetization, the latter two curves are very close. The highest value R_g at the lowest T is observed for a chain that contains a small-particle segment in the middle. In Fig. 4(b) the T dependence of R_g for two types of Y-like SMP structures is shown. In a purely monodisperse case (gray circles), R_g first decreases slowly on cooling, reaching the local minimum at $T \sim 0.7$, where its magnetization exhibits a local minimum as well. Then, similarly to the magnetic moment,
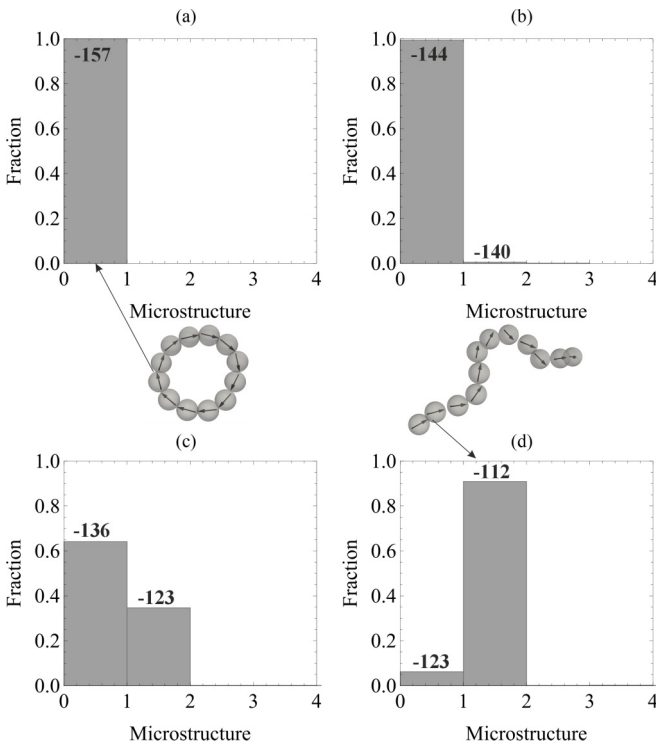

FIG. 5. Microstate probability histogram for a monodisperse linear SMP structure at (a) $T = 0.20$, (b) $T = 0.70$, (c) $T = 1.00$, and (d) $T = 1.50$. Arrows from the configurations sketched in the middle point to corresponding bins.
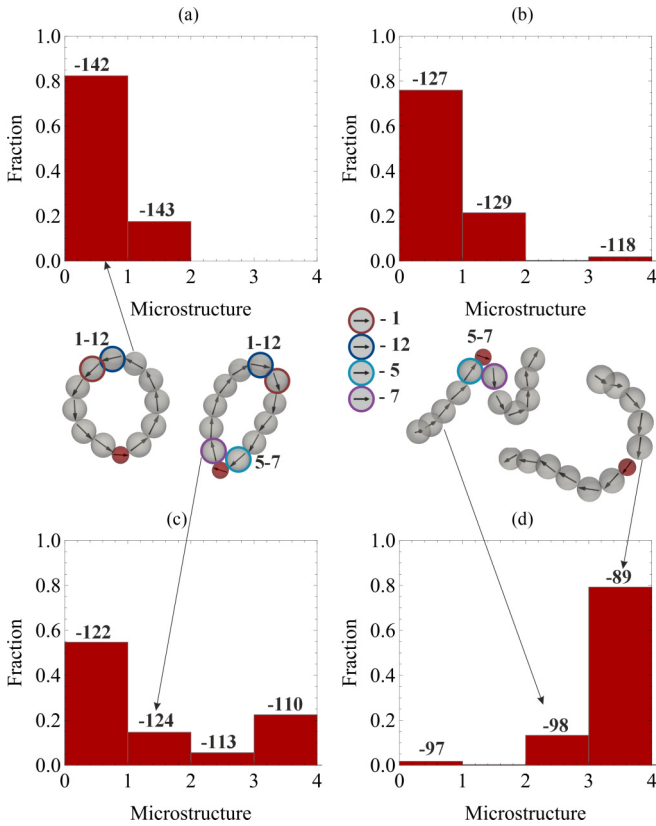
FIG. 6. Microstate probability histogram for a linear SMP structure with one small particle in the middle at (a) $T = 0.20$, (b) $T = 0.80$, (c) $T = 1.00$, and (d) $T = 2.00$. Particles are numbered as shown in the legend. Each microstate is characterized by the set of nonpermanent bonds provided next to the actual conformation. Arrows from the conformations point to corresponding bins along the horizontal axes.

FIG. 7. Microstate probability histogram for a linear SMP structure with one small particle at the end at (a) $T = 0.20$, (b) $T = 0.35$, (c) $T = 0.60$, and (d) $T = 1.00$. Particles are numbered as shown in the legend. Each microstate is characterized by the set of nonpermanent bonds provided next to the actual conformation. Arrows from the conformations point to corresponding bins along the horizontal axes.

R_g effectively grows a little with a subsequent decrease of T, shows a local maximum at $T \sim 0.5$, and decays rapidly for lower temperatures. This last rapid decrease of R_g is not observed for a Y-shaped SMP structure with a small-particle arm (cyan squares) for the temperature range studied here. A milder decrease for a Y-shaped SMP structure with a small particle arm can however be foreseen for lower T. For the rest of the temperature interval investigated here, the behavior is similar to its monodisperse counterpart. Looking at gray circles in Fig. 4(c), showing the values of R_g for a monodisperse X-shaped SMP structure, we notice overall similarities with the curve for a monodisperse Y-shaped SMP structure, albeit with a less pronounce decay for $T < 0.5$. If the X-shaped SMP structure has a small-particle arm, in agreement with its magnetic moment, no local maximum is found on cooling, but rather a little shoulder at $T \sim 0.5$. As previously observed for the total magnetic moment in Fig. 3(d), gyration radii of ringlike SMP structures plotted in Fig. 4(d) exhibit qualitatively different behavior from the other three topologies. Here, on cooling, R_g monotonically grows, independently of the presence of small particles, and converges to an ideal nonperturbed ring made of corresponding numbers of small and large particles.
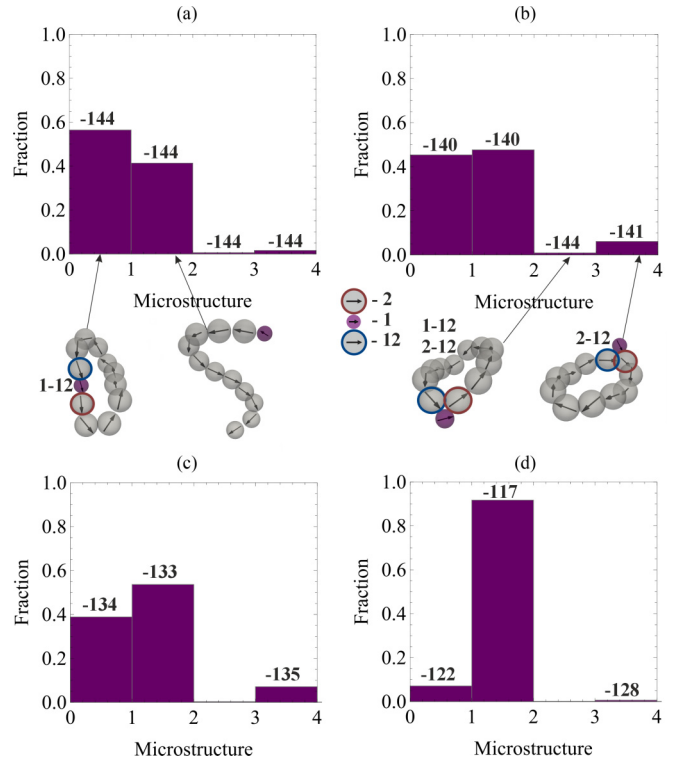
Both total magnetization and gyration radius are integral characteristics and reflect the macroscopic behavior of SMP structures, but their complex behavior found above must be the consequence of the microscopic structural transitions that various SMP structures undergo on cooling. In order to elucidate those microscopic details, in the next session we study the changes in the neighborhood of each monomer caused by cooling.

B. Structural transitions

We expect that on cooling, along with permanent FENE links between neighboring monomers, an extra nonpermanent bond will be formed. Below, to form a new bond we require two nonpermanently bonded particles to be at a distance $0.65(\sigma_i + \sigma_j)$ and have a negative value of magnetic dipolar interaction. We number all particles in each SMP structure so that we can analyze monomers with which numbers are most likely to bond. Each combination of pairs of numbers, bond array, corresponds to a given microstate for the SMP structure. Going through 1000 snapshots for each SMP structure, we build the distribution of most probable microstates (bond arrays) at each temperature and present them in the form of occurrence frequency histograms illustrated in the following sections. Since it is impossible to plot every histogram for every SMP type, we focus on the temperatures at which R_g
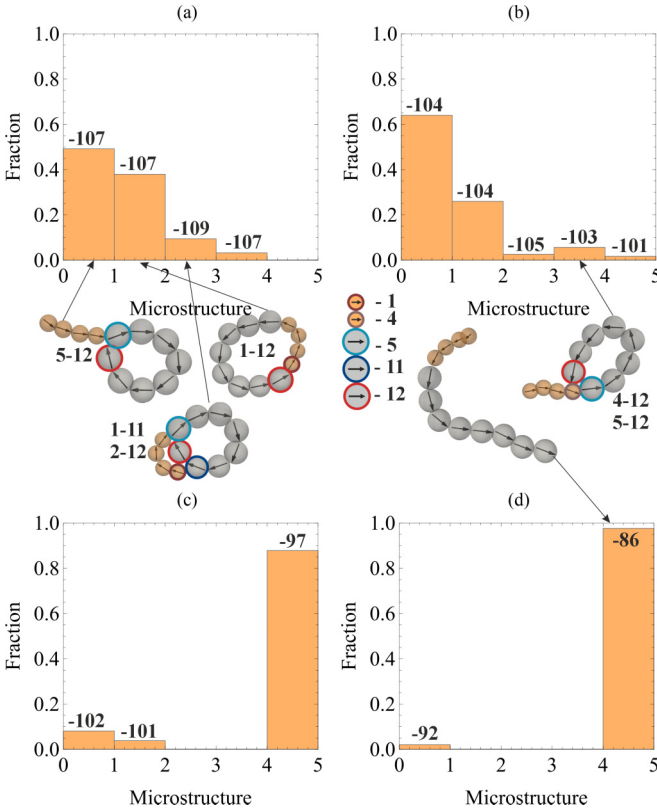
FIG. 8. Microstate probability histogram for a linear SMP structure with four small particle at the end at (a) $T = 0.20$, (b) $T = 0.35$, (c) $T = 0.47$, and (d) $T = 1.00$. Particles are numbered as shown in the legend. Each microstate is characterized by the set of nonpermanent bonds provided next to the actual conformation. Arrows from the conformations point to corresponding bins along the horizontal axes.

FIG. 9. Microstate probability histogram for a linear SMP structure with four small particle in the middle of the chain at (a) $T = 0.20$, (b) $T = 0.80$, (c) $T = 1.20$, and (d) $T = 1.60$. Particles are numbered as shown in the legend. Each microstate is characterized by the set of nonpermanent bonds provided next to the actual conformation. Arrows from the conformations point to corresponding bins along the horizontal axes.

and magnetization exhibit qualitative changes such as minima, maxima, or inflection points. In order to understand if a given microstate dominates because of its energy or entropy, each frequency of the microstate in the histograms is accompanied by the corresponding magnetic energies calculated as the average over all SMP structures in a given configuration.

1. Chainlike SMP structures

Looking at monodisperse linear SMP magnetization and R_g, we can see a monotonic decrease of both observables on cooling up to $T \sim 0.7$. For lower temperature no particular changes are observed. In fact, in this temperature regime there is only one microstate and it is a ring as shown in Figs. 5(a) and 5(b). The probability of a chain growing with T and ring microstates is clearly rare for $T > 1$ [see Fig. 5(c)]. Importantly, an open chain is energetically less favorable for any T, but at high temperatures the entropy gained by the chain's open ends overpowers the energetic advantage of a ring.

The number of available microstates for a linear SMP structure with one small particle in the middle is much higher, as shown in Fig. 6. Here, at low temperature $T = 0.2$ [Fig. 6(a)], along with a ring configuration created by bonding end large particles 1 and 12, two large particle neighbors of a small one, numbered 5 and 7, might also form a bond, lead-
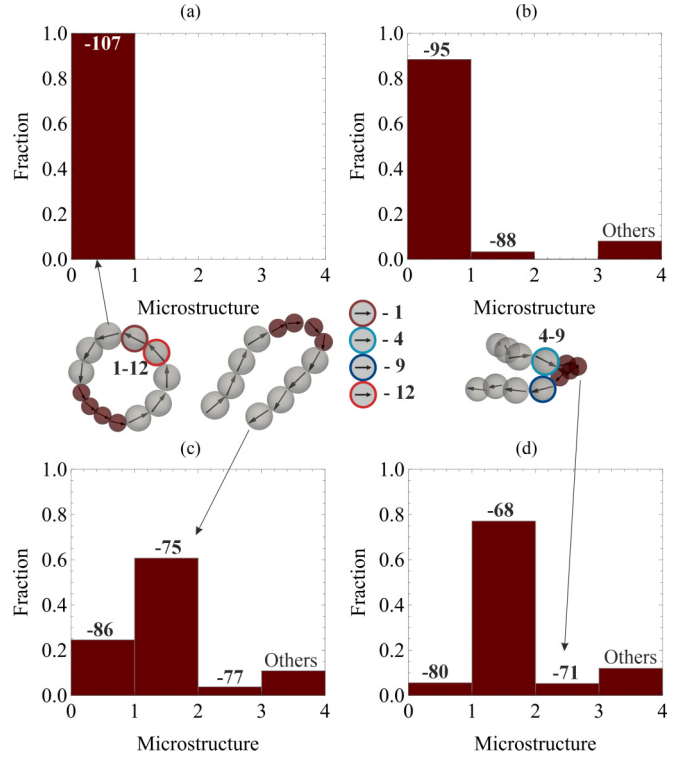
ing to a more squeezed elongated configuration. The energy gained by forming the 5-7 bond in a closed ring configuration and a relatively large configurational phase space in which such a bond can form makes the probability of the latter microstate grow slightly if temperature grows [see Fig. 6(b), where $T = 0.8$]. For higher T [Figs. 6(c) and 6(d)], however, fully open structures prevail, in which neighbors of a small particle remain nonbonded.

Microstates collected in Fig. 7 explain the existence of a local maximum of R_g and magnetization observed for linear SMP structure with one small particle at the end at T around unity: Even at low T an open configuration remains highly probable. The tendency to close the magnetic flux in turn is reflected by two microstates similar to those observed for a SMP structure with one small particle in the middle, namely, a ring, where a small particle is squeezed out by its large neighbors numbered 2 and 12, albeit with much lower probability for the SMP structure with a small particle at the end. Here the gain from forming a 1-12 bond is on average negligible and basically all configurations observed have very similar magnetic energies. A small particle at the end of the chain makes closed conformations unstable. Indeed, despite the conformations in microstate 2 in Fig. 6 and in microstate 3 in Fig. 7 being identical, the probability of finding them is defined by the gain of forming a nonpermanent bond: If
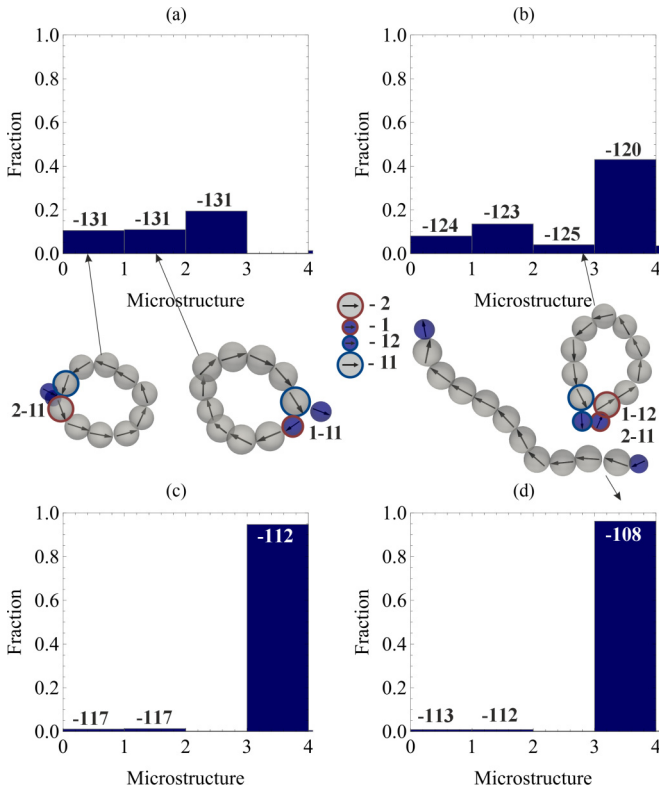
FIG. 10. Microstate probability histogram for a linear SMP structure with two small particles at the ends at (a) $T = 0.20$, (b) $T = 0.50$, (c) $T = 0.80$, and (d) $T = 1.00$. Each microstate is characterized by the set of nonpermanent bonds provided next to the actual conformation. Arrows from the conformations point to corresponding bins along the horizontal axes.
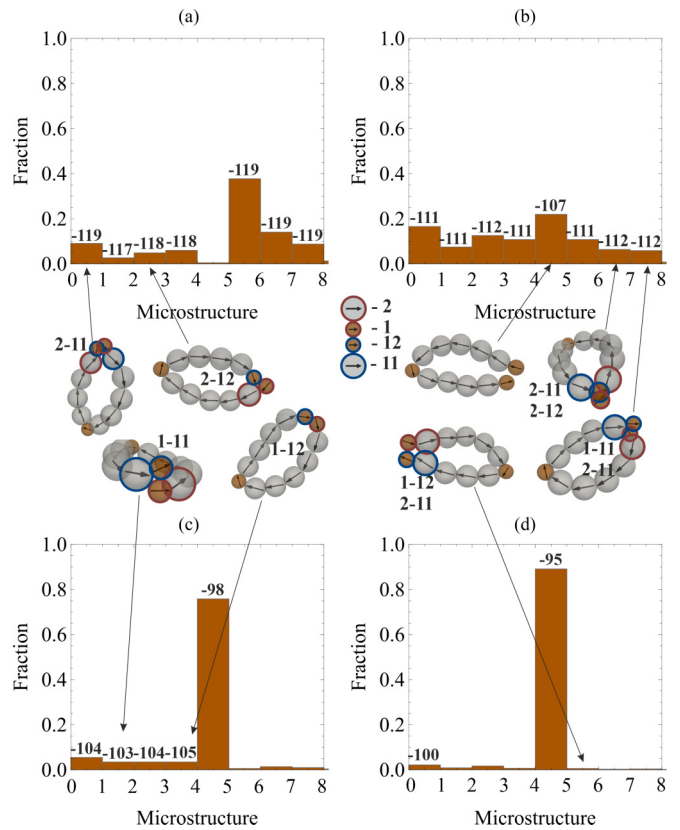

FIG. 11. Microstate probability histogram for a linear SMP structure with three small particles, two at the ends and one in the middle, at (a) $T = 0.20$, (b) $T = 0.50$, (c) $T = 0.80$, and (d) $T = 1.00$. Each microstate is characterized by the set of nonpermanent bonds provided next to the actual conformation. Arrows from the conformations point to corresponding bins along the horizontal axes.

a small particle is at the end this bond is less advantageous than in the case of the two large particles connecting.

If instead of one particle a small-particle segment forms an open chain end, as shown in Fig. 8, the energetic proximity of the conformations remains, but an open structure at low T is replaced by a ring made of large particles only (bond 5-12) with a small-particle segment being depleted. This configuration explains the very high maxima in R_g and total magnetization detected in the previous section. An interesting conformation here that arises at low T is the one in which bonds 2-12 and 1-11 are formed. It minimizes the magnetic energy, but has a very low configurational entropy, so it never dominates.

If the small-particle segment is in the middle of the chain, the conformations shown in Fig. 9 are qualitatively similar to those observed in Fig. 6. Weak segments promote squeezed configurations at high T, but the ring with only one nonpermanent bond 1-12 dominates for $T < 1$.

As it is seen in Fig. 10, if two small particles are at the end, the probability of finding a closed structure decreases in comparison to Fig. 7, even if all possible configurations with bonds between particles 1, 2, 11, and 12 are summed up. In fact, the magnetic energies of all conformations are very close.

In contrast, if one small particle is added also in the middle, it creates a weak point in a linear SMP structure, where it is likely to bend. Such a bending leads to the formation of

various squeezed rings, as illustrated in Fig. 11. It also adds a clear split in magnetic energies. The presence of those rings manifests through the decrease of R_g and magnetization on cooling that is more similar to the SMP structures with only one small particle at the end.

2. Y-like SMP structures

Monodisperse Y-like SMP structures, as shown in Fig. 12, gradually bond the free ends to each other on cooling. Due to high configurational entropy, there is a vast range of microstates whose probability is rather low. We collect all of those microstates with probabilities below 5% into one group, labeled "Others" here and in the following figures. For temperatures above one, not shown in Fig. 12, the most probable configuration is the structure with three open ends, whose magnetization and R_g are basically constant. One can see that for $T \sim 0.7$, the two arms close, forming a racketlike conformation. The handle of the racket is not stretched first, as entropy dominates. This is the point where R_g reaches its local minimum. Further cooling leads to the competition between the energetic gain of closing the third arm to form a fully closed structure and the configurational entropy. At the same time, dipolar interactions lead to the straightening of the free arm, and here R_g approaches its local maximum.
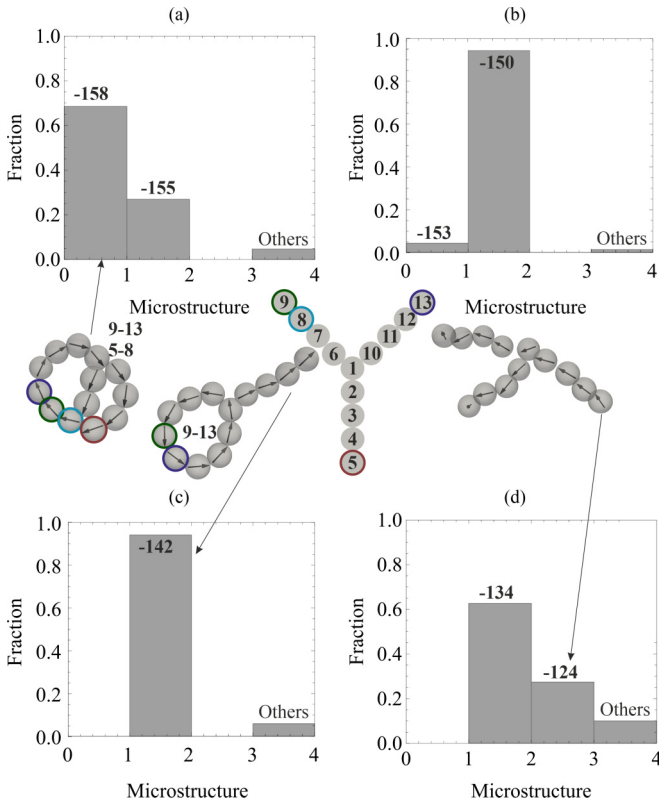
FIG. 12. Microstate probability histogram for a Y-like SMP structure with no small particles at (a) $T = 0.20$, (b) $T = 0.40$, (c) $T = 0.70$, and (d) $T = 1.00$. Each microstate is characterized by the set of nonpermanent bonds provided next to the actual conformation. Arrows from the conformations point to corresponding bins along the horizontal axes.

At $T = 0.20$, basically the only remaining conformation is a closed basketlike structure, whose magnetization has a finite value, due to the fact that one arm cannot be fully compensated by the other two that are forming a ring with zero dipole moment.

Once one of the SMP structure arms is replaced by its small-particle counterpart, the full closure is less probable, as shown in Fig. 13. Large-particle free ends, particles 9 and 13, bond at relatively high $T \sim 0.6$, while the small-particle arm remains in a linear configuration. At this point R_g shows a local minimum. Since for the closure of the small arm lower temperatures are required, the increase of the gyration radius observed on further cooling is related to the stretching of the small-particle arm in order to optimize dipolar interactions. The relative magnetization decrease on cooling for a bidisperse Y-like SMP structure is much larger than for a monodisperse case, as the small-particle arm has a much smaller contribution to the overall magnetization of the structure. In general, conformations found at low T here are very similar to those in Fig. 8.

3. X-like SMP structures

At low T, X-like monodisperse SMP structures form quasispherical configurations, closing all four arms so that two orthogonal rings are formed. Such conformations have several
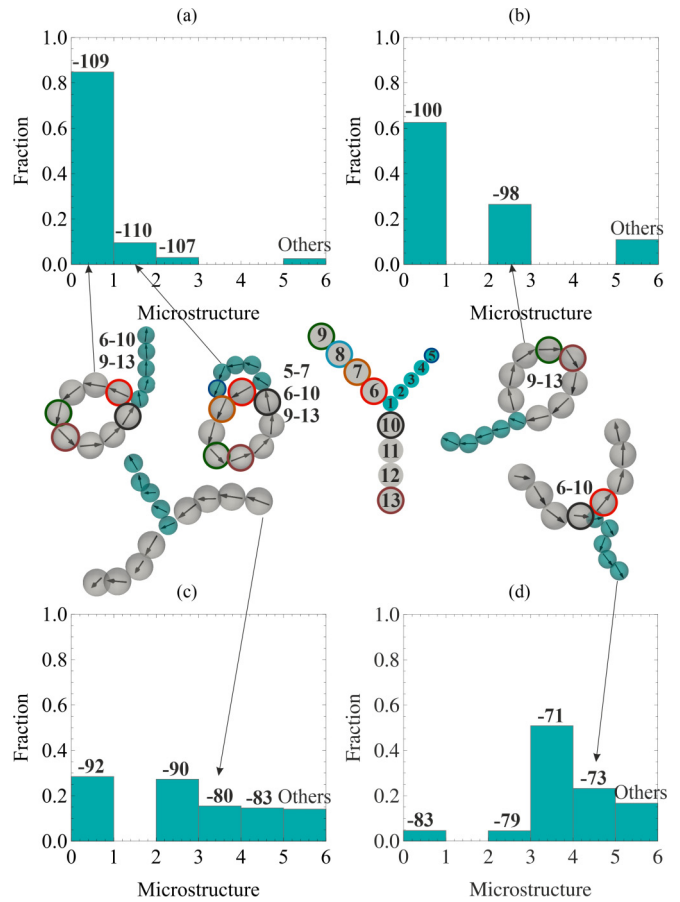

FIG. 13. Microstate probability histogram for a Y-like SMP structure with a small particle arm at (a) $T = 0.20$, (b) $T = 0.60$, (c) $T = 1.00$, and (d) $T = 1.50$. Each microstate is characterized by the set of nonpermanent bonds provided next to the actual conformation. Arrows from the conformations point to corresponding bins along the horizontal axes.

realizations, as shown in Fig. 14(a). These realizations have a low R_g and practically zero magnetization. For $T \sim 0.35$ the local maximum of R_g shown with gray circles in Fig. 4(c) is reached. This corresponds to Fig. 14(b), which shows that the maximum is related to the opening of the two rings into an 8-like conformation. The local minimum of the R_g at $T \sim 0.6$ is due to strong fluctuations of an 8-like conformation before it breaks at $T \sim 1$, first into one ring and two free arms and then into a fully open structure. Interestingly, all the closed or semiclosed conformations here have on average very similar magnetic energies.

Surprisingly enough, if one arm of an X-like SMP structure is formed by small particles, the number of probable microstates decreases. On cooling, an open structure first closes two large-particle arms as seen in Fig. 15(c) and then leaves only a small-particle arm open at $T \sim 0.6$ (compare to chains with a small-particle segment in Fig. 8 at the end and Y-like SMP structures with a small-particle arm in Fig. 13). Finally, at $T \sim 0.2$ shown in Fig. 15(a), the full closure into the most energetically advantageous conformation takes place. This row of rather simple structural transformations leads to a monotonic decrease of both magnetization and R_g on
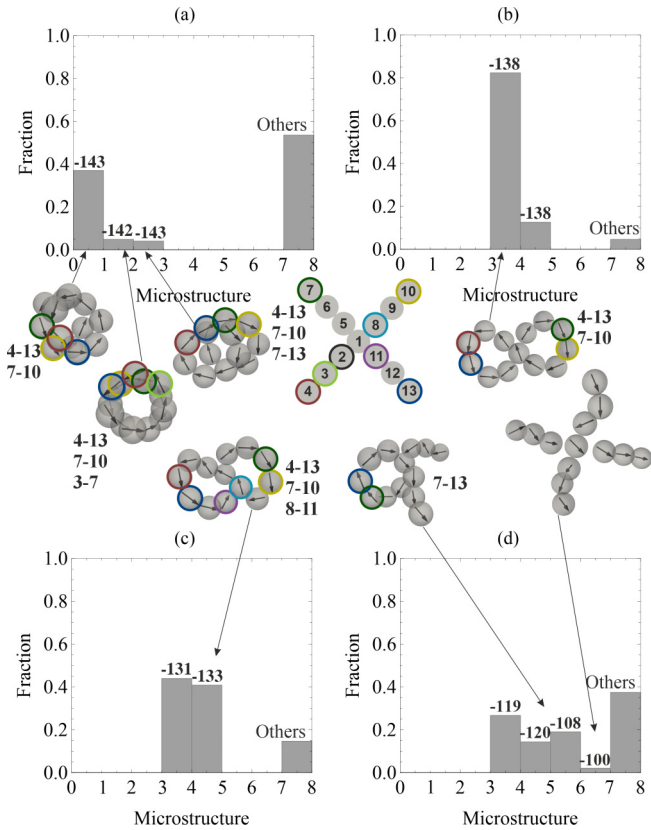
FIG. 14. Microstate probability histogram for an X-like SMP structure with no small particles at (a) $T = 0.20$, (b) $T = 0.35$, (c) $T = 0.60$, and (d) $T = 1.00$. Each microstate is characterized by the set of nonpermanent bonds provided next to the actual conformation. Arrows from the conformations point to corresponding bins along the horizontal axes.

FIG. 15. Microstate probability histogram for an X-like SMP structure with a small particle arm at (a) $T = 0.20$, (b) $T = 0.35$, (c) $T = 0.60$, and (d) $T = 1.00$. Each microstate is characterized by the set of nonpermanent bonds provided next to the actual conformation. Arrows from the conformations point to corresponding bins along the horizontal axes.

cooling. The only peculiarity here is related to $T \sim 0.60$, as the stretching of the only free small-particle arm gives rise to a shoulder in magnetization [see the dark green squares in Fig. 3(c)].

4. Ringlike SMP structures

For the case of monodisperse ringlike SMP structures, the situation is very simple and is not plotted here: At high T the ring fluctuates and can form an extra bond between nonpermanently connected particles, but already from $T \sim 1$ the ring tends to be very regular. Its magnetization monotonically decreases and the value of R_g approaches that of an ideal ring.

For a ringlike SMP structure with a single six-small-particle segment, the variety of microstates is not high, as shown in Fig. 16, and the energies of those conformations are found to be very similar. At high T the ring fluctuates, particularly the segment made of small particles. In Fig. 3(d) we observed that this type of ring is the only one whose magnetic moment grows on cooling, starting from $T \sim 1.5$. It turns out to be energetically advantageous for a small-particle segment to stretch, forming basically a straight line, and for a large-particle segment to bend in the middle, thus leading to an almost triangular conformation.
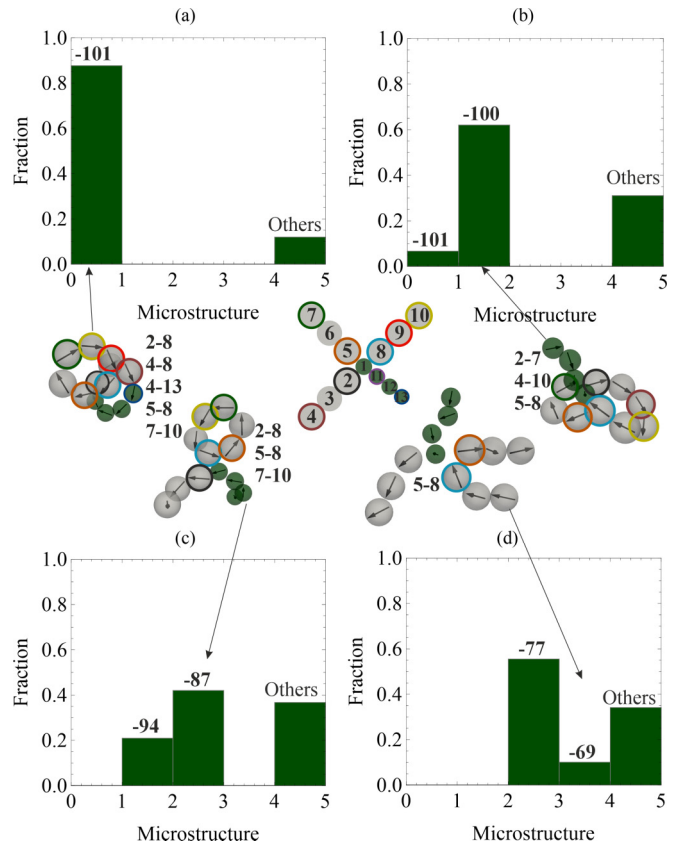
For rings made of alternating three-particle segments, a microstate corresponding to no extra bonds remains dominant because of its high entropy up to $T \sim 0.5$, albeit having a slightly higher magnetic energy. As it is shown in Fig. 17, however, already at $T = 2.00$ [Fig. 17(d)], large-particle segments start stretching, forming antiparallel linear configurations that turn out to compensate for the energy loss caused by a strong bending of small-particle segments. The tendency to form antiparallel bonds strengthens on cooling. At the lowest temperature all antiparallel pairs of large particles can be formed as in Fig. 17(a) and the first bin in it.

IV. CONCLUSION

In this work, using molecular dynamics computer simulations combined with parallel tempering, we investigated structural transitions and macroscopic properties of supramolecular magnetic polymerlike structures of four different topologies, i.e., linear and Y-like, X-like, and ringlike, containing monomers of two different sizes on cooling. This general model allows us not only to analyze the influence of temperature and polydispersity, but also to find the most probable structures that SMP structures with strongly interacting monomers can form. It is the combination of the magnetic
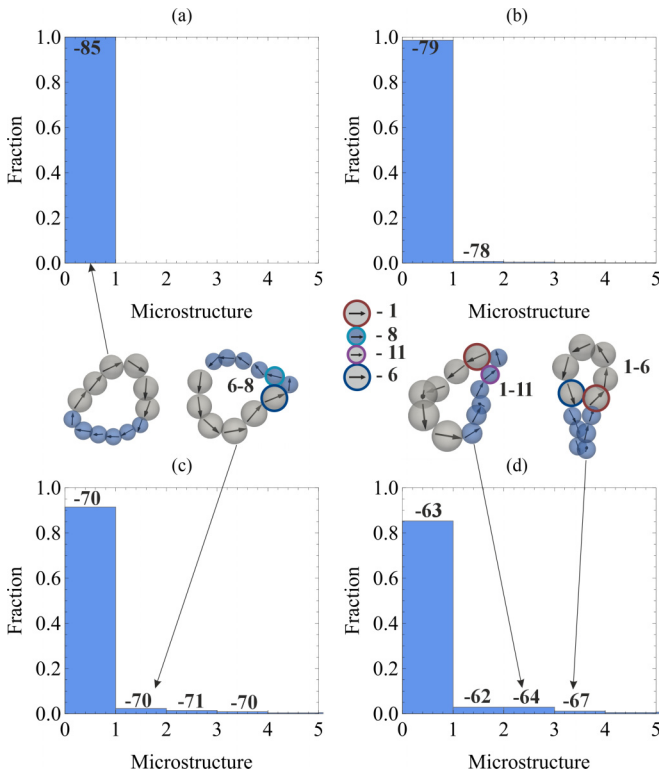
FIG. 16. Microstate probability histogram for a ringlike SMP structure with a small six-particle segment at (a) $T = 0.20$, (b) $T = 0.50$, (c) $T = 1.00$, and (d) $T = 1.50$. Each microstate is characterized by the set of nonpermanent bonds provided next to the actual conformation.

FIG. 17. Microstate probability histogram for a ringlike SMP structure with alternating small and large three-particle segments at (a) $T = 0.20$, (b) $T = 0.50$, (c) $T = 1.00$, and (d) $T = 2.00$. Each microstate is characterized by the set of nonpermanent bonds provided next to the actual conformation.

moment and the structure of SMP structures that makes it suitable to be used as an effective magnetically controllable container for directed transport, be that in medicine or nanofluidics.

In order to classify the structures, we introduced the numbering of microstates on the basis of monomer bonds analysis. To each independent microstate we attributed a vector of nonpermanent bond formed inside a SMP structure of a certain topology and granulometric composition at a given temperature.

Our findings revealed that the presence of small particles dramatically changes not only the structural transitions happening in magnetic SMP structures on cooling, but also affects the magnetic response of those systems. The simplest example is a linear SMP structure with one small particle in the middle. This small particle becomes a weak point near which the whole structure bends and as a result the closure transition occurs at higher temperature than for a monodisperse linear SMP structure. At the same time, if two small particles are at the ends of a linear SMP structure, much lower temperature is required in order for a chain to close into a ring. Despite the fact that bidisperse Y-like SMP structures rarely form a fully closed conformation, even at very low temperature, the small-particle arm keeps hanging and the magnetic moment of the monodisperse Y's is found to not decrease as for a bidisperse case. The reason for that is the formation of a basketlike structure made of three large-particle arms. In such
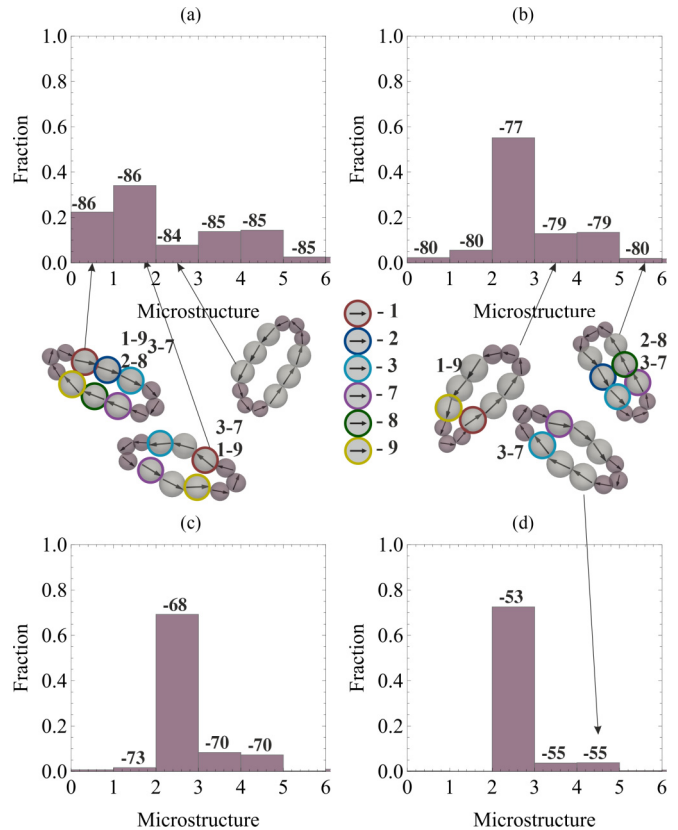
a conformation the magnetic compensation of two arms only is possible, while the third arm will still have a remanent magnetic moment. Thus, regardless a very low gyration radius and the absence of free ends, a monodisperse Y-like SMP structure at low temperature has a remanent magnetization. The situation with X-like SMP structures is opposite: Monodisperse X's close at relatively high temperatures into 8-like structures that on further cooling transform into a three-dimensional structure formed by two orthogonal rings. The magnetic moment of such structures is negligible. In contrast, a bidisperse X-like SMP structure first closes its three large-particle arms, leaving a small-particle arm to hang. It results in a slower decay of the magnetization and the gyration radius on cooling if compared to the monodisperse X. Finally, we found that if a large-particle ringlike SMP structure has a single segment made of small particles, on cooling, instead of a perfect ring, which is observed for a monodisperse case, a triangular conformation is assumed, in which a small-particle segment is fully stretched. As an outcome, with a temperature decrease, an unexpected growth of magnetization for such a ringlike structure is observed. If a ring has two small-particle segments separated by large-particle ones, the latter tend to align antiparallel, forming a narrow elongated compact structure with zero magnetization.

A general conclusion is that the small particles effectively shift the closure of the magnetic flux inside the SMP

structures to either higher temperatures if trapped in the middle of the structure or to lower ones if forming an open end. In both configurations, small particles lead to the increase of the configurational entropy. Even though the structures investigated here might seem too idealized, we expect the qualitative conclusions to hold if magnetic moments are not coupled with the backbone or if the polydispersity inside the structures does not follow the strict rules considered above. The reason for that is our recent study of linear nanopolymers with superparamagnetic particles [47], where we showed that the field response of the structure primarily depends on the cross-linking and is only weakly affected by the internal degrees of freedom of that particle magnetic moment. It is worth mentioning here that restricting the latter

degrees of freedom became possible with recently proposed DNA-origami-based filaments [48]. The next step would be to investigate the influence of magnetic fields and hydrodynamic flows on the selected structures in order to elucidate the stability.

ACKNOWLEDGMENTS

[1] A. C. Balazs, T. Emrick, and T. P. Russell, Science **314**, 1107 (2006).

[2] D. Alexandrov and A. Zubarev, Philos. Trans. R. Soc. A **377**, 20180353 (2019).

[3] S. L. Biswal and A. P. Gast, Anal. Chem. **76**, 6448 (2004).

[4] T. Yang, T. O. Tasci, K. B. Neeves, N. Wu, and D. W. Marr, Langmuir **33**, 5932 (2017).

[5] R. Tietze, J. Zaloga, H. Unterweger, S. Lyer, R. P. Friedrich, C. Janko, M. Pöttler, S. Dürr, and C. Alexiou, Biochem. Biophys. Res. Commun. **468**, 463 (2015).

[6] E. M. Furst, C. Suzuki, M. Fermigier, and A. P. Gast, Langmuir **14**, 7334 (1998).

[7] E. M. Furst and A. P. Gast, Phys. Rev. Lett. **82**, 4130 (1999).

[8] C. Goubault, P. Jop, M. Fermigier, J. Baudry, E. Bertrand, and J. Bibette, Phys. Rev. Lett. **91**, 260802 (2003).

[9] L. Cohen-Tannoudji, E. Bertrand, L. Bressy, C. Goubault, J. Baudry, J. Klein, J. F. Joanny, and J. Bibette, Phys. Rev. Lett. **94**, 038301 (2005).

[10] H. Singh, P. E. Laibinis, and T. A. Hatton, Langmuir **21**, 11500 (2005).

[11] H. Singh, P. E. Laibinis, and T. A. Hatton, Nano Lett. **5**, 2149 (2005).

[12] F. Martínez-Pedrero, M. Tirado-Miranda, A. Schmitt, and J. Callejas-Fernández, Phys. Rev. E **76**, 011405 (2007).

[13] B. A. Evans, A. R. Shields, R. L. Carroll, S. Washburn, M. R. Falvo, and R. Superfine, Nano Lett. **7**, 1428 (2007).

[14] J. J. Benkoski, S. E. Bowles, R. L. Jones, J. F. Douglas, J. Pyun, and A. Karim, J. Polym. Sci. B **46**, 2267 (2008).

[15] Z. Zhou, G. Liu, and D. Han, ACS Nano **3**, 165 (2009).

[16] J. J. Benkoski, J. L. Breidenich, O. M. Uy, A. T. Hayes, R. M. Deacon, H. B. Land, J. M. Spicer, P. Y. Keng, and J. Pyun, J. Mater. Chem. **21**, 7314 (2011).

[17] H. Wang, Y. Yu, Y. Sun, and Q. Chen, Nano **06**, 1 (2011).

[18] D. Sarkar and M. Mandal, J. Phys. Chem. C **116**, 3227 (2012).

[19] J. L. Breidenich, M. C. Wei, G. V. Clatterbaugh, J. J. Benkoski, P. Y. Keng, and J. Pyun, Soft Matter **8**, 5334 (2012).

[20] E. Busseron, Y. Ruff, E. Moulin, and N. Giuseppone, Nanoscale **5**, 7098 (2013).

[21] J. Byrom, P. Han, M. Savory, and S. L. Biswal, Langmuir **30**, 9045 (2014).

[22] L. J. Hill and J. Pyun, ACS Appl. Mater. Interfaces **6**, 6022 (2014).

[23] M. B. Bannwarth, S. Utech, S. Ebert, D. A. Weitz, D. Crespy, and K. Landfester, ACS Nano **9**, 2720 (2015).

[24] R. Dreyfus, J. Baudry, M. L. Roper, M. Fermigier, H. A. Stone, and J. Bibette, Nature (London) **437**, 862 (2005).

[25] Y. Xiong, Q. Chen, N. Tao, J. Ye, J. Tang, J. Feng, and X. Gu, Nanotechnology **18**, 345301 (2007).

[26] F. Zhang and C.-C. Wang, J. Phys. Chem. C **112**, 15151 (2008).

[27] M. Ma, Q. Zhang, J. Dou, H. Zhang, D. Yin, W. Geng, and Y. Zhou, J. Colloid Interface Sci. **374**, 339 (2012).

[28] B. Bharti, A.-L. Fameau, M. Rubinstein, and O. D. Velev, Nat. Mater. **14**, 1104 (2015).

[29] S. Kralj and D. Makovec, ACS Nano **9**, 9700 (2015).

[30] M. Bennet, L. Bertinetti, R. K. Neely, A. Schertel, A. Körnig, C. Flors, F. D. Müller, D. Schüler, S. Klumpp, and D. Faivre, Faraday Discuss. **181**, 71 (2015).

[31] É. Bereczk-Tompa, F. Vonderviszt, B. Horváth, I. Szalai, and M. Pósfai, Nanoscale **9**, 15062 (2017).

[32] S. H. Xu, G. T. Fei, H. M. Ouyang, Y. Zhang, P. C. Huo, and L. De Zhang, J. Mater. Chem. C **3**, 2072 (2015).

[33] A. Hosseinifar, M. Shariaty-Niassar, S. Seyyed Ebrahimi, and M. Moshref-Javadi, Langmuir **33**, 14728 (2017).

[34] X. Wen, L. Gu, and A. M. Bittner, Z. Phys. Chem. **232**, 1631 (2018).

[35] Z. Lin, H. Emamy, B. Minevich, Y. Xiong, S. Xiang, S. Kumar, Y. Ke, and O. Gang, J. Am. Chem. Soc. **142**, 17531 (2020).

[36] A. Cebers, J. Phys.: Condens. Matter **15**, S1335 (2003).

[37] V. P. Shcherbakov and M. Winklhofer, Phys. Rev. E **70**, 061803 (2004).

[38] A. Cēbers and I. Javaitis, Phys. Rev. E **69**, 021404 (2004).

[39] A. Cēbers, Curr. Opin. Colloid Interface Sci. **10**, 167 (2005).

[40] M. Belovs and A. Cēbers, Phys. Rev. E **73**, 051503 (2006).

[41] A. Cēbers and T. Cīrulis, Phys. Rev. E **76**, 031504 (2007).

[42] K. Ērglis, D. Zhulenkovs, A. Sharipo, and A. Cēbers, J. Phys.: Condens. Matter **20**, 204107 (2008).

[43] A. Cebers and K. Erglis, Adv. Funct. Mater. **26**, 3783 (2016).

[44] P. A. Sánchez, J. J. Cerda, V. Ballenegger, T. Sintes, O. Piro, and C. Holm, Soft Matter **7**, 1809 (2011).

[45] P. A. Sánchez, J. J. Cerdà, T. Sintes, and C. Holm, J. Chem. Phys. **139**, 044904 (2013).

[46] A. A. Kuznetsov, J. Magn. Magn. Mater. **470**, 28 (2019).

[47] D. Mostarac, P. A. Sánchez, and S. Kantorovich, Nanoscale **12**, 13933 (2020).

[48] Y. Xiong, Z. Lin, D. Mostarac, B. Minevich, Q. Peng, G. Zhu, P. A. Sánchez, S. Kantorovich, Y. Ke, and O. Gang, Nano Lett. **21**, 10547 (2021).

[49] P. A. Sánchez, E. S. Pyanzina, E. V. Novak, J. J. Cerdà, T. Sintes, and S. S. Kantorovich, Macromolecules **48**, 7658 (2015).

[50] D. Lüsebrink, J. J. Cerdà, P. A. Sánchez, S. S. Kantorovich, and T. Sintes, J. Chem. Phys. **145**, 234902 (2016).

[51] E. Novak, E. Pyanzina, D. Rozhkov, M. Ronti, J. Cerdà, T. Sintes, P. Sánchez, and S. Kantorovich, J. Mol. Liquids **271**, 631 (2018).

[52] E. Novak, E. Pyanzina, D. Rozhkov, P. Sánchez, and S. Kantorovich, J. Magn. Magn. Mater. **470**, 22 (2019).

[53] V. Russier, C. de Montferrand, Y. Lalatonne, and L. Motte, J. Appl. Phys. **112**, 073926 (2012).

[54] C. Munoz-Menendez, I. Conde-Leboran, D. Baldomir, O. Chubykalo-Fesenko, and D. Serantes, Phys. Chem. Chem. Phys. **17**, 27812 (2015).

[55] T. I. Becker, O. V. Stolbov, D. Y. Borin, K. Zimmermann, and Y. L. Raikher, Smart Mater. Struct. **29**, 075034 (2020).

[56] M. V. Avdeev, J. Mol. Liquids **189**, 68 (2014).

[57] A. O. Ivanov, Z. Wang, and C. Holm, Phys. Rev. E **69**, 031206 (2004).

[58] R. Saldivar-Guerrero, R. Richter, I. Rehberg, N. Aksel, L. Heymann, and O. S. Rodriguez-Fernández, J. Chem. Phys. **125**, 084907 (2006).

[59] L. Fischer and A. M. Menzel, Smart Mater. Struct. **30**, 014003 (2021).

[60] A. Leschhorn, M. Lücke, C. Hoffmann, and S. Altmeyer, Phys. Rev. E **79**, 036308 (2009).

[61] G. M. Range and S. H. L. Klapp, Phys. Rev. E **70**, 061407 (2004).

[62] S. Kantorovich, J. J. Cerdà, and C. Holm, Phys. Chem. Chem. Phys. **10**, 1883 (2008).

[63] A. B. Dobroserdova and S. S. Kantorovich, Phys. Rev. E **103**, 012612 (2021).

[64] S. Kantorovich, A. O. Ivanov, L. Rovigatti, J. M. Tavares, and F. Sciortino, Phys. Rev. Lett. **110**, 148306 (2013).

[65] J. D. Weeks, D. Chandler, and H. C. Andersen, J. Chem. Phys. **54**, 5237 (1971).

[66] G. S. Grest and K. Kremer, Phys. Rev. A **33**, 3628 (1986).

[67] A. Arnold, O. Lenz, S. Kesselheim, R. Weeber, F. Fahrenberger, D. Roehm, P. Košovan, and C. Holm, in *Meshfree Methods for Partial Differential Equations VI*, edited by M. Griebel and M. A. Schweitzer, Lecture Notes in Computational Science and Engineering Vol. 89 (Springer, Berlin, 2013), pp. 1–23.

[68] J. J. Cerdà, S. Kantorovich, and C. Holm, J. Phys.: Condens. Matter **20**, 204125 (2008).

[69] M. P. Allen and D. J. Tildesley, *Computer Simulation of Liquids*, 1st ed. (Clarendon Press, Oxford, 1987).

[70] Y. Sugita and Y. Okamoto, Chem. Phys. Lett. **314**, 141 (1999).

[71] A. Mitsutake, Y. Sugita, and Y. Okamoto, Peptide Sci. **60**, 96 (2001).